Evolution of aerosol chemistry in Xi'an, inland China during the dust storm period of 2013−Part 1. Sources, chemical forms and formation mechanisms of nitrate and sulfate

Ge Hui Wang[1,2]*, Chun Lei Cheng[1,3], Yao Huang[1,3], Jun Tao[4], Yan Qin Ren[1,3], Feng Wu[1], Jing Jing Meng[1,3], Jian Jun Li[1], Yu Ting Cheng[1,3], Jun Ji Cao[1], Sui Xin Liu[1], Ting Zhang[1], Rong Zhang[1], Yu Bao Chen[1]

[1]State Key Laboratory of Loess and Quaternary Geology, Institute of Earth Environment, Chinese Academy of Sciences, Xi'an 710075, China
[2]School of Human Settlements and Civil Engineering, Xi'an Jiaotong University, Xi'an 710079, China
[3]University of Chinese Academy of Sciences, Beijing 100049, China
[4]South China Institute of Environmental Science, Guangzhou 510655, China

*Corresponding author: Prof. Ge Hui Wang, wanggh@ieecas.cn
Tel: 86-29-8832-9320, Fax: 86-29-8832-0456.

Abstract: Total suspended particulate (TSP) sample was hourly collected in Xi'an, an inland mega-city of China near the Loess Plateau, during a dust storm event of 2013 (9 March 18:00−12 March 10:00 LT), along with a size-resolved aerosol sampling and an online measurement of $PM_{2.5}$. The TSP and size-resolved samples were determined for EC, OC, water-soluble organic carbon (WSOC) and nitrogen (WSON), inorganic ions and elements to investigate chemistry evolution of dust particles. Hourly concentrations of Cl^-, NO_3^-, SO_4^{2-}, Na^+ and Ca^{2+} in the TSP samples reached up to 34, 12, 180, 72 and 28 $\mu g\ m^{-3}$, respectively, when dust peak arrived over Xi'an. Chemical compositions of the TSP samples showed that during the whole observation period NH_4^+ and NO_3^- linearly correlated each other (r^2=0.76) with a molar ratio of 1:1, while SO_4^{2-} and Cl^- well correlated with Na^+, Ca^{2+}, Mg^{2+} and K^+ (r^2>0.85). Size distributions of NH_4^+ and NO_3^- presented a same pattern, which dominated in the coarse mode (>2.1μ m) during the event and predominated in the fine mode (<2.1μm) during the non-event. SO_4^{2-} and Cl^- also dominated in the coarse mode during the event hours, but both exhibited two equivalent peaks in the fine and coarse modes during the non-event, respectively, due to the fine mode accumulations of secondarily produced SO_4^{2-} and biomass burning emitted Cl^- and the coarse mode enrichments of urban soil-derived SO_4^{2-} and Cl^-. Linear fit regression analysis further indicated that SO_4^{2-} and Cl^- in the dust samples possibly exist as Na_2SO_4, $CaSO_4$ and NaCl, which directly originated from Gobi desert surface soil, while NH_4^+ and NO_3^- in the dust samples exist as NH_4NO_3. We propose a mechanism to explain these observations in which aqueous phase of dust particle surface is formed via uptake of water vapor by hygroscopic salts such as Na_2SO_4 and NaCl, followed by heterogeneous formation of nitrate on the liquid phase and subsequent absorption of ammonia. Our data indicate that 54±20% and 60±23% of NH_4^+ and NO_3^- during the dust period were secondarily produced via this pathway with the remaining derived from Gobi desert and Loess Plateau while SO_4^{2-} in the event almost entirely originated from the desert regions. Such cases are different from those in the East Asian continental outflow region, where during the Asia dust storm events SO_4^{2-} is secondarily produced and

62 concentrates in sub-micrometer particles as $(NH_4)_2SO_4$ and/or NH_4HSO_4. To the best of our

63 knowledge, the current work for the first time revealed an infant state of East Asian dust ageing

64 process in the regions near the source, which is helpful for researchers to understand the panorama

65 of East Asian dust ageing process from the desert area to the downwind region.

66 **Key words:** Heterogeneous reactions; Size distributions; Origins and formation mechanisms;

67 Mineralogy and hygroscopicity; Production speed.

68

69

70 **1. Introduction**

71 　　Mineral dust is the largest contributor to particulate matter in the atmosphere with estimated

72 annual emission fluxes of 1000−3000 Tg (average, 1840 Tg) at present day (Dentener et al., 1996,

73 2006; Ginoux et al., 2001). Dust particles can influence the solar radiation directly by scattering

74 sunlight and indirectly by acting as cloud condensation nuclei (CCN) and ice nuclei (IN) (Buseck

75 and Pósfai, 1999; Formenti et al., 2011; Manktelow et al., 2010). Gobi deserts of northern China

76 and Mongolia and the Taklimakan desert of western China are the major source regions of East

77 Asian dust (McNaughton et al., 2009; Mochida et al., 2007). Modeling results indicate that around

78 100−460 Tg yr^{-1} of dust is emitted annually from the East Asia source regions (Laura et al, 2006)

79 and transport eastwardly, exerting a significant impact on the atmosphere over the downwind

80 regions including east coastal China (Arimoto et al., 2006; Kim et al., 2004; Li et al., 2014; Li and

81 Shao, 2009; Sun et al., 2010; Wang et al., 2013; Wang et al., 2012), Korea (Geng et al., 2014;

82 Song et al., 2013; Sullivian et al., 2007), Japan (Takahashi et al., 2011; Tobo et al., 2010; Uno et al.,

83 2009), and northwest America (Huebert et al., 2003; Leaitch et al., 2009; McNaughton et al., 2009;

84 Parrington et al., 1983; Singh et al., 2009). A recent study found that dust from Sahara and Asia

85 transport over Pacific Ocean and increase the snow precipitation in mountainous areas of Nevada,

86 USA (Creamean et al., 2013). In addition to the impact on climate, dust storm also affect marine

87 productivity because dust-bonded iron, nitrogen and phosphorus are the important nutrients to

88 marine microbes (Boyd et al., 2007; Duce et al., 2008; Jickells et al., 2005; Kanakidou et al., 2012;

89 Zamora et al., 2011, 2013).

90   Due to rapid urbanization and industrialization in China, annual consumption of coal has

91 increased to 3.61 billion tons in the country recently (China Statistic Press, 2010), along with a

92 sharp increase in vehicle numbers, resulting in high burden of SO_2, NOx, EC, organic matter,

93 nitrate, sulfate, and other pollutants in the atmosphere over China (Geng et al., 2014; He, 2014;

94 Huang et al., 2014; van Donkelaar et al., 2010; Wang et al., 2014). During the long-range transport

95 dust can become coated with nitrate, sulfate, ammonium and other pollutants, leading to a series of

96 changes in dust behavior in the atmosphere such as water uptake, deposition, and scattering

97 sunlight (Boreddy et al., 2014; Creamean et al., 2013; Formenti et al., 2011; Grassian, 2001;

98 Seinfeld et al., 2004; Sullivan et al., 2009). Studies found that SO_2 level in the atmosphere of China

99 has become stable and even decreased since 2006 because Chinese government has promulgated a

100 strict standard on SO_2 emission (Lu et al., 2010; Menon et al., 2008; Wang et al., 2013). As a result,

101 atmospheric sulfate aerosol loading has been decreasing in many Chinese urban regions since 2006,

102 whereas NOx and particulate nitrate levels have kept stable and even increased (Wang et al., 2011,

103 2012, 2013; Zhang et al., 2009). Due to the chemical affinity of nitrogen oxides and nitric acid with

104 dust particles (Hanisch and Crowley, 2001; Mogili et al., 2006; Saliba and Chamseddine, 2012;

105 Song et al., 2013; Usher et al., 2003), such a change in the atmospheric environment of China

106 suggests that dust particle behavior might also be changing compared to the situations ten years ago.

107 Therefore, it is necessary to investigate the present physicochemical properties of airborne particles

108 in the country during dusty periods.

109   In the past decades, numerous observations have been conducted along the Asian dust

110 transport pathways including east coastal China, Korea, Japan, Pacific Ocean and northwest

111 America to investigate the ageing process of East Asian dust during the long-range transport

112   (Huebert et al., 2003; Kim et al., 2004). On contrast, only a few field measurements have been done

113   in the upstream regions especially inland cities of China (Arimoto et al., 2004; Huang et al., 2010),

114   where the dust particle ageing could be at the infant state due to the proximity of the source regions

115   including deserts and Loess Plateau. Xi'an is a mega-city in inland China, which is located at the

116   south edge of Loess Plateau. High level of particle pollution has been a persistent problem in the

117   city (Shen et al., 2008). In comparison with that (55 $\mu g\ m^{-3}$, unpublished data) in 1997 the annual

118   level (27 $\mu g\ m^{-3}$, unpublished data) of sulfate of $PM_{2.5}$ of the city in 2012 has decreased by a factor

119   of around two due to the SO_2 emission control, while NOx and nitrate have increased about 25%.

120   Acidic gas concentration is a key factor affecting heterogeneous reaction rates of dust particle with

121   SO_2, NOx and HNO_3 (g), apart from relative humidity, temperature and dust mineralogy and

122   morphology. For example, calcite ($CaCO_3$), which is a common component of East Asian dust and

123   accounts for 3.6−21% of the dust mass (Liu, l985), can rapidly convert to $Ca(NO_3)_2$ less than 3 min

124   under 1 ppbv HNO_3 (g) but longer than 4 hr under low HNO_3 (g) mixing ratio (10 pptv) (Sullivan

125   et al., 2009). Since $Ca(NO_3)_2$ is highly hygroscopic, the chemically modified dust can absorb water

126   vapor and form a liquid phase on the surface (Li et al., 2014). Therefore, changes in

127   physicochemical properties of dust particles occur and are probably much more significant than

128   before due to the recent increase in NOx emission. In order to investigate the impact of dust storm

129   on the downwind aerosol chemistry under the current high level of NOx and relatively low level of

130   SO_2 conditions, we performed an intensive filter-based sampling with a 1h time resolution to

131   investigate chemical evolution of urban airborne particles in Xi'an in the period of 9−12 March

132   2013, during which the annual heaviest dust storm passed through the city with an hourly

133   maximum of TSP more than 7000 $\mu g\ m^{-3}$. In the current work, we focus on the changes in aerosol

134   chemistry specifically nitrate and sulfate during the event. We first investigated the composition

135   and size distribution of airborne particles in the event and compared with those in the non-event to

136   discuss the chemical evolution of dust particles. Then we identified the chemical forms of nitrates

137 and sulfates existing in the dust to explore their sources and formation mechanisms. We found for

138 the first time an enrichment of ammonium nitrate in the dust particles, which is different from a

139 fine mode accumulation of ammonium sulfate in Asia continental outflow region such as northwest

140 Pacific and northwest America. Our results further revealed that such a phenomenon is relevant to

141 the water-soluble components of mineral dusts, which consist of hygroscopic salts (e.g., NaCl and

142 Na_2SO_4) and originate from dried salt lakes in western China and Gobi deserts.

143 **2. Experimental section**

144 **2.1 Collections of TSP and size-resolved samples**

145 TSP samples were hourly collected at an airflow rate of 1.0 m^3 min^{-1} from 9 March

146 18:00−12 March 10:00 LT by using two air samplers TCH-1000 (Tianhong Company, China) on

147 the rooftop of a three-story building on the campus of Institute of Earth Environment, CAS, which

148 is located in the downtown area of Xi'an. Simultaneously, size-segregated samples were also

149 collected with each set lasting for 3 hr during the dust storm period and 12 hr during the non-dust

150 period by using two size-resolved samplers (Series 20-800, Thermo Electron Corporation USA).

151 The cutoff points of the size-segregated samples are 0.43, 0.65, 1.1, 2.1, 3.3, 4.7, 5.8 and 9.0 μm at

152 an airflow rate of 28.3 L min^{-1}. All the samples were collected onto pre-combusted quartz filters

153 (450 ^{o}C for 6 hr). Field blank samplers were also collected at the beginning and the end of the

154 sampling campaign by mounting pre-baked blank filters onto the samplers for about 10 min without

155 sucking any air. After sampling, all the filters were individually sealed in aluminum foil bags and

156 stored at −20 ^{o}C prior to analysis. A total of 65 TSP samples and six sets of size-segregated

157 samples were collected. In addition to the above filter-based sampling, online measurement of

158 $PM_{2.5}$ was also conducted by using E-BAM-9800 analyzer (Met One, USA).

159 **2.2 Analyses of TSP and size-resolved samples**

160 **2.2.1 Inorganic ions, water-soluble organic (WSOC) and inorganic carbon (WSIC), and**

161 **water-soluble organic nitrogen (WSON)**

162   Aliquot (size: 12.56 cm^2) of the filter was cut into pieces and extracted for three times with

163   Milli-Q pure water under sonication. One part of the combined water-extracts was determined for

164   inorganic ions using Dionex-6000 ion chromatography. Another part of the water-extracts was

165   determined for water-soluble organic carbon (WSOC), water-soluble inorganic carbon (WSIC) and

166   water-soluble total nitrogen (WSTN) using Shimadzu 5000 TOC/N Analyzer. The detailed analysis

167   methods for inorganic ions, WSOC and WSTN can be found elsewhere (Wang et al., 2010). NO_3^-

168   and NH_4^+ are the major water-soluble inorganic nitrogen (WSIN) species in airborne particles, thus

169   the difference between WSTN and WSIN is defined as water-soluble organic nitrogen (WSON).

170   **2.2.2 Organic carbon (OC) and elemental carbon (EC)**

171   OC and EC in the TSP samples were measured by a DRI Model 2001 Carbon Analyzer

172   using the Interagency Monitoring of Protected Visual Environments (IMPROVE) thermal/optical

173   reflectance (TOR) protocol. Briefly, a size of 0.53 cm^2 filter was put in a quartz boat inside the

174   analyzer and progressively heated to temperatures of 120 $^{\circ}$C, 250 $^{\circ}$C, 450 $^{\circ}$C, and 550 $^{\circ}$C in a non-

175   oxidizing helium (He) atmosphere, and 550 $^{\circ}$C, 700 $^{\circ}$C, and 800 $^{\circ}$C in an oxidizing atmosphere

176   containing 2% oxygen in helium.

177   **2.2.3 Elements**

178   Elements of the TSP samples were determined by Energy Dispersive X-Ray Fluorescence

179   (ED-XRF) spectrometry (Epsilon 5 ED-XRF, PANalytical B. V., Netherlands). The X-ray source is

180   a side window X-ray tube with a gadolinium anode and operated at an accelerating voltage of

181   25e100 kV and a current of 0.5e24 mA (maximum power: 600 W). The characteristic X-ray

182   radiation is detected by a germanium detector (PAN 32). Each sample was analyzed for 30 min to

183   obtain a spectrum of X-ray counts versus photon energy with the individual peak energies matching

184   specific elements and peak areas corresponding to elemental concentrations. The spectrometer was

185   calibrated with thin-film standards obtained from MicroMatter Co. (Arlington, WA, USA). In the

186   current study, 14 elements (i.e., S, Cl, K, Ca, Ti, Mn, Fe, Zn, Cr, Ni, As, Br, Mo, Pb) were

187   determined. The element concentrations for blank quartz fiber filter are 0.00−0.66 µg cm^{-2} and

188   lower than 10% of those in the TSP samples.

3. Results and discussion

190   During the sampling period a massive dust storm event originating from Mongolia Gobi

191   desert arrived over Xi'an on 9 March with a highest TSP level of 7527 µg m^{-3} at the beginning hour

192   (18:00 LT) and a second peak at 10 March 13:00. From 9 March 18:00 to 10 March 21:00 LT TSP

193   level decreased from the highest to less than 1000 µg m^{-3} that is a typical level of TSP in X'an

194   during spring. A 48-hr backward trajectory analysis indicated a three-phase pattern for the

195   movements of air masses arrived in Xi'an during the sampling period. As seen in Fig. 1, the 48-hr

196   backward trajectories showed that from 9 March 18:00 to 10 March 21:00 air parcels originated

197   from Gobi deserts of Mongolia and North China and directly moved to Xi'an at 100 m, 300 m and

198   500 m levels above the ground along the same tracks. TSP within this period ranged from

199   774−7527 µg m^{-3} with an average of 2109±1360 µg m^{-3}. We classified this period as dust storm

200   event (Phase I, see Fig. 1a and b for examples). From 10 March 21:00 to 11 March 12:00 LT air

201   parcels at the 100 m and 300 m levels still originated from the Gobi deserts but moved to east

202   coastal China first and then returned to Xi'an, while the 500 m air parcel originated from southern

203   China and moved slowly to Xi'an after spanned over Qinling Mountain (Fig. 1c and e). During this

204   period the TSP level ranged from 412 to 1037 µg m^{-3} with an average of 630±155 µg m^{-3} (Table 1,

205   hereinafter). We classified this period as transition period (Phase II, see Fig. 1c for example). After

206   11 March 12:00, the three levels of air parcels originated from North China Plain and moved to

207   Xi'an from Qinling Mountain (about 1500 m above the ground level, Fig. 1d and e). During this

208   period the TSP varied from 476−1399 µg m^{-3} with an average of 687±194 µg m^{-3}. We classified

209   this period as non-dust storm period (Phase III, see Fig. 1d for example). As seen in Fig. 1e, Xi'an

210   is located in Guanzhong Basin and very close to Qinling Mountain. From the transport tracks it can

211   be seen that air parcels within the Phase III moved much slower in comparison with those in Phase

212 I and Phase II. Thus, we believe that aerosols in the non-dust storm period are mostly derived from

213 the local sources rather than from long-range transport. In the following sections we will discuss

214 the aerosol chemistry evolution based on the three classified categories.

215 **3. 1 Hourly changes in chemical compositions of ambient particles**

216 As shown in Fig. 2a, during the dust storm period TSP showed two maxima with the largest

217 peak at the first hour (i.e., 9 March 18:00 LT) and a second peak at the noon time (11:00−13:00 LT)

218 of 10 March. At the same time $PM_{2.5}$ concentration was 152 ± 127 μg m^{-3} with a maximum of 621

219 μg m^{-3} occurring at the first hour (Fig. 2a). As shown Table 1, relative abundances of $PM_{2.5}$/TSP

220 were $7.4\pm3.4\%$, $14\pm2.3\%$, and $23\pm4.8\%$ during the dust storm event, transition period and non-dust

221 storm event, respectively, suggesting that surface soils in Gobi deserts and Loess Plateau consist of

222 a certain amount of fine particles. From the backward trajectories we found that air parcels at the

223 first ten hours directly moved across the Guanzhong Basin from the north to the south (as

224 exemplified in Fig. 1a), sweeping pollutants out of Xi'an. Then, the air mass moved to Xi'an from

225 it's east neighborhood at 10 March 10:00 LT (see Fig. 1b for an example) with pollutants

226 originating from the upwind cities such as Weinan and Huayin. As a result, EC was almost

227 undetectable at the beginning ten hours but sharply increased to more than 30 μg m^{-3} at the 10

228 March noon time during the dust storm period (Fig. 2b).

229 Total inorganic ions in the dust storm, transition and non-dust storm periods accounted for

230 4%, 8% and 12% of the TSP mass, respectively (Fig. 3). In contrast, relative abundance of WSOC

231 to OC at the three periods gradually decreased from 0.4 in the dust period to 0.3 in the non-dust

232 period (Fig. 3), which is lower than that (0.5 ± 0.1) observed for dust storm events in the spring of

233 2009 (Wang et al., 2013). Our previous studies found that dusts from Gobi deserts contain

234 significant amounts of water-soluble organic compounds, e.g., trehalose (Wang et al., 2011, 2012).

235 In addition, heterogeneous formation of secondary organic aerosols (SOA) on dust surface is

236 another important contributor to WSOC of dust (Sullivan and Prather, 2007; Wang et al., 2013).

237   Therefore, in comparison with that in 2009 spring the lower ratio of WSOC/OC is most likely due

238   to the differences in the dust source regions and/or SOA formation on the dust surface. OC/EC ratio

239   presented similar values during the transition and non-dust periods with an average value around

240   4.0, which is higher than that for $PM_{2.5}$ in the city since coarse particles contain less amount of

241   elemental carbon. Our previous investigation on the impact of Asian dust storm on Xi'an aerosols

242   in the spring of 2009 found that 88% (in mass) of airborne particulate sulfate originated from Gobi

243   desert soil in the presence of the dust storm (Wang et al., 2011, 2013). A recent study on the

244   atmospheric aerosols collected in Taklimakan desert also reported that airborne particles in the

245   desert are abundant in sulfate, which accounts for about 4% the particle mass with no significant

246   difference for particles with different sizes (Wu et al., 2012). WSOC/WSON ratios are higher in the

247   dust storm and transition periods and lower in the non-dust period, which can be ascribed to more

248   WSON species emitted from anthropogenic sources such as agricultural fertilizer and livestock

249   dejecta (Cape et al., 2011; Chen et al., 2010; Wang et al., 2010).

250   As shown in Fig. 4a, extremely high levels of sulfate were observed during the dust storm

251   period (Phase I) with a peak of 180 μg m^{-3} at the first hour, accounting for 2.3% of the TSP mass

252   (Table 1), which falls in the range reported for the airborne dust in Taklimakan desert by Wu et al

253   (2012). Due to the second peak of dust storm arrived in Xi'an at the noon of 10 March, SO_4^{2-}

254   concentration showed a moderate peak as did TSP (see the inserted figure in Fig. 4a). During the

255   whole sampling period NO_3^- and NH_4^+ concentrations displayed similar variation patterns, which

256   are different from other ions and are almost continuously increasing from the dust storm period to

257   the non-dust storm period (Fig. 4b). Temporal variation pattern of Cl^- is similar to that of SO_4^{2-},

258   while the variation pattern of F^- is similar to EC, indicating that Cl^- and SO_4^{2-} are of similar natural

259   origins but F^- and EC are of common anthropogenic sources, e.g., coal combustion (Wang et al.,

260   2010). There are many dried salt lakes in north and west parts of China and Gobi area of Mongolia,

261   in which halite (NaCl), gypsum ($CaSO_4 \bullet 2H_2O$), mirabilite($Na_2SO_4 \bullet 10H_2O$) and other salts are

262   common components of the surface soil (Zheng, 1991). Mineral species containing calcium and

263   magnesium often co-exist in desert regions. For example, dolomite ($CaMg(CO_3)_2$) is a common

264   mineral salt in surface soil in Taklimakan, Gobi desert and Loess Plateau of China (Li et al., 2007;

265   Maher et al., 2009). Thus, both presented the same temporal pattern during the dust and transition

266   periods when dust particles from the above regions are dominant (Fig. 4d). However, Ca^{2+} and

267   Mg^{2+} displayed divergent patterns in the non-dust storm period when the aerosols are dominated by

268   local sources, indicating both ions are of different origins.

269   As seen in Fig. 5a, relative abundance of elemental calcium to TSP (Ca/TSP) during the

270   whole sampling period was nearly constant, which slightly increased from 6.9±1.0% in the event to

271   8.2±1.4% in the non-event. In contrast, ratio of Ca^{2+}/Ca was keeping increase from 7.1±2.8% in the

272   event, 16±6.0% in the transition period to 22±5.7% in the non-event, indicating an enrichment of

273   local soil that consists of more water-soluble calcium and/or a continuous conversion of elemental

274   calcium into calcium cation. Although the mass ratio of SO_4^{2-}/TSP displayed an increasing trend

275   from about 1.0% during the dust storm event to about 5.0% in the non-event, the ratios of SO_4^{2-}-S/

276   total-S in the TSP samples during the three periods are almost the same (Fig. 5b), which are

277   62±13% in the dust storm event, 61±6.1% in the transition time, and 54±5.2%, in the non-event

278   period, respectively, suggesting that sulfate in the samples is largely derived from dust/soil and

279   photochemical production of sulfate was minor even in the non-dust period. Such a result is

280   consistent with the observation for the dust storm during the spring of 2009, by which we found

281   only 12% of particulate sulfate in Xi'an at that time was formed by secondary oxidation and 88%

282   of the sulfate was transported from the desert region (Wang et al., 2013).

283   **3.2 Size distributions**

284   Size is an important parameter of an aerosol, which is related to its origin, formation

285   pathway and composition (Hinds, 1999). To further investigate the chemical evolution process of

286   the urban aerosols, size-resolved chemical compositions were analyzed for the dust storm and non-

287   dust storm periods. The size-segregated samples collected in the transition period were not used in

288   this study because sampling duration of these samples overlapped somewhat with the non-dust

289   period. As shown in Fig. 6a, Cl^- presented a bimodal pattern in the dust storm period with a large

290   peak in the coarse mode (>2.1 μm) and a minor peak in the fine mode (<2.1 μm), in contrast to the

291   case in the non-dust storm period, which is characterized by two equivalent peaks in the fine and

292   coarse modes, respectively. The pronounced coarse mode peak in the dust storm period further

293   suggests the origin of NaCl from dried salt lakes in the Gobi desert region. NO_3^- and SO_4^{2-}

294   dominated in the coarse mode when dust was present, but in the non-dust storm period nitrate in the

295   fine mode was much more abundant than in the coarse mode while sulfate displayed two equivalent

296   peaks in both modes (Fig. 6b and c). The SO_4^{2-} distribution patterns in the dust storm and non-dust

297   storm periods are similar to those of Cl^-, while NO_3^- displayed similar patterns to those of NH_4^+ in

298   both periods (Fig. 6b−d). During the non-dust storm period Cl^-, NO_3^- and SO_4^{2-} in the fine mode

299   (<2.1 μm) accounted for 55%, 58% and 54% of the mass in the whole size range, respectively

300   (Table 2). Whereas in the dust event the fine modes of Cl^-, NO_3^- and SO_4^{2-} decreased significantly,

301   accounting for 40±4%, 31±6% and 27±7% of the total, respectively (Table 2).

302   Size distribution patterns of Na^+ are almost identical with those of Cl^- in both the dust and

303   non-dust storm periods (Fig. 6a and e), probably indicating that both ions have the same sources

304   even in the non-dust storm period. Apart from dried salt lakes, soil and seal salt, Na^+ and Cl^- can

305   also originate from biomass burning. For examples, Andreae et al (1998) measured aerosol

306   emissions from savanna fires in southern Africa and found that Na^+, Cl^- and K^+ were abundant in

307   the smoke with 40−90% of the mass distributing in particles with a diameter less than 1.2 μm. K^+

308   is generally considered a tracer of biomass burning smoke and enriched in fine particles (Andreae

309   et al., 1998; Shen et al., 2007; Wang et al., 2012), thus the fine mode (<2.1 μm) of K^+ was

310   relatively low in the dust storm period, accounting for 40±7% of the total mass in the whole size

311   range, and became predominant in the non-dust storm period, accounting for 66% of the total (Fig.

312   6f and Table 2). Such a result is consistent with the observation by Shen at al. (2008), which

313   reported that Cl^- and K^+ in the urban air of Xi'an are enriched in fine particles (i.e., $PM_{2.5}$) and

314   largely derived from extensively burning wheat straw and maize stalks by farmers in the suburban

315   areas for cooking and heating. Since Mg^{2+} and Ca^{2+} are largely derived from soil, both dominated

316   in the coarse mode during the dust and non-dust periods (Fig. 6g and h).

317   **3.3 Chemical forms, sources and productions of nitrate and sulfate**

318   Fig. 7 shows the linear fit regressions for nitrate, sulfate, ammonium and other major

319   cations in the TSP samples during the dust storm and transition periods. Nitrate showed a robust

320   correlation with ammonium (r^2=0.76, Fig. 7a) but presented no correlation with the sum of Na^+, K^+,

321   Mg^{2+} plus Ca^{2+} (Fig. 7b). On the contrary, sulfate during the dust storm and transition periods did

322   not correlate with ammonium but strongly correlated with the sum of the above cations (Fig. 7c and

323   d). Interestingly, robust linear correlations (r^2>0.99) were found for the samples collected at the

324   beginning three hours (red dots in Fig. 7a−d), suggesting that dust particles in the city within this

325   period are of the same chemical compositions and are not chemically modified. Nitrate and

326   ammonium mass concentrations not only displayed the similar size distribution patterns during the

327   whole sampling period but also strongly linearly correlated each other during the dust storm and

328   transition periods with a slope of 0.28 that is equal to the 1:1 molar ratio of NH_4^+ to NO_3^- (Fig. 7a).

329   Therefore, we assumed that NH_4NO_3 is the major chemical form of both ions in the airborne

330   particles, especially in the dust storm and transition periods. Equivalent percentages showed that

331   Na^+ and Ca^{2+} are the two major cations during the dust storm and transition periods, accounting for

332   77±5.0% (range, 65−87%) of the total cation equivalent (Fig. 8a). Nitrate and sulfate are the two

333   major anions, accounting for 86±2.1% (range, 80−90%) of the total anion equivalent (Fig. 8b). As

334   discussed above, NaCl and NH_4NO_3 are the major chemical forms of Cl^- and NO_3^- in the TSP

335   samples, respectively. Thus, it is reasonably expected that the remaining Na^+ and other major

336   cations in the samples exist as sulfate salts (i.e., Na_2SO_4, $CaSO_4$, $MgSO_4$ and K_2SO_4) during the

337   dust storm and transition periods. Concentrations of these sulfate salts during the dust and transition

338   periods and their relative abundances to the total sulfate in the water-soluble fraction are

339   summarized in Table 3 and shown in Fig. 9. Within these periods Na_2SO_4 and $CaSO_4$ are the major

340   sulfate salts, which originate from dust source regions and account for more than 90% of the total

341   water-soluble sulfate salts.

342   Fig. 10a shows a temporal variation in molar ratio of NO_3^-/SO_4^{2-} during the whole period.

343   Because nitrate in Gobi desert surface soil is much less than sulfate, the molar ratio of NO_3^- to SO_4^{2-}

344   at the beginning hours was <0.1 and gradually increased up to 2.8 along with an increase in the

345   observation time (see Fig. 10a), indicating that the heterogeneous formation of NO_3^- on dust surface

346   is much faster than SO_4^{2-}. For example, during the nighttime of 9 March and 10 March molar ratio

347   of NO_3^-/SO_4^{2-} increased by a rate of 0.07 hr^{-1} (Fig. 10b). As discussed above dust particles at the

348   first three hours during the dust storm period were not chemically modified, and EC at that time

349   was zero. Thus, here we use the first sample as a reference to calculate the heterogeneous

350   productions of NO_3^-, SO_4^{2-} and NH_4^+ for the remaining TSP samples by using the following

351   equation.

$$dA = C_A^i - \frac{C_A^{ref}}{C_{TSP}^{ref}} \times C_{TSP}^i$$

352

353   Where dA is the secondarily formed NO_3^-, SO_4^{2-} or NH_4^+ in the sample i, C_A^i is the concentration

354   of NO_3^-, SO_4^{2-} or NH_4^+ in the sample i, C_A^{ref} is the concentration of NO_3^-, SO_4^{2-} or NH_4^+ in the first

355   sample at the beginning hour of the dust storm period, C_{TSP}^{ref} is the TSP concentration of the first

356   sample, and C_{TSP}^i is the TSP concentration of the sample i.

357   The calculated results, i.e., dNO_3^-, dSO_4^{2-} and dNH_4^+, are produced by heterogeneous

358   reactions of HNO_3 (g), NOx, SO_2 and NH_3 on the dust surface and are normalized by the total. As

359   seen in Fig. 11, $dNO_3^-/total-NO_3^-$ and $dNH_4^+/total-NH_4^+$ presented identical variation patterns with

360   a sharp increase from less than 0.1 to 0.9 in the dust storm and transition periods and then to above

361   0.9 in the non-dust period. However, the ratio of dSO_4^{2-}/total-SO_4^{2-} is almost zero in the dust storm

362   and transition periods and increased to about 0.4 at the late hours of the non-dust storm period.

363   Such phenomena again demonstrate that nitrate and ammonium in the airborne particles during the

364   whole campaign existed as the chemical form of NH_4NO_3 and its production speed is much faster

365   than sulfate. In the dust storm period SO_4^{2-} almost entirely originated from surface soil in Gobi

366   desert and no significant amount of SO_4^{2-} in the dust storm event was secondarily produced (Fig.

367   11).

368   Hygroscopicity of the ambient aerosols during the whole campaign was also investigated by

369   determining the hygroscopic growth factor of the water-soluble fraction of the TSP samples (Huang

370   and Wang, 2014). The results showed that κ value of the water-soluble fraction of dust particles

371   ranged from 0.20−0.38 (0.30±0.04), indicating a wettable nature of the dust particles (Andreae and

372   Rosenfeld, 2008). Here, we propose a three-step mechanism of heterogeneous formation of nitrate

373   on dust surface to explain the above secondary formation of NH_4NO_3 (see Fig. 12). As discussed

374   above, the airborne particles during the dust storm and transition period consist of significant

375   amounts of water-soluble NaCl and Na_2SO_4. These compounds are very hygroscopic and thus may

376   take up water vapor, forming a liquid phase on the dust surface even under the low RH conditions

377   of the dust storm period (RH=22±3.5%, Table 1). The aqueous phase is favorable for the formation

378   of NH_4NO_3, which is probably formed via a gas-phase homogeneous reaction of nitric acid with

379   ammonia and a subsequent partitioning into the liquid phase (Nie et al., 2012; Pathak et al., 2011).

380   In addition, NO_3^- can also be produced in the liquid phase via heterogeneous reactions of gaseous

381   HNO_3, N_2O_5 and NO_x with dust particles (Finlayson-Pitts et al., 2003; Hanisch and Crowley, 2001;

382   Laskin et al., 2005; Usher et al., 2003), followed by a subsequent absorption of the gas-phase NH_3

383   to form NH_4NO_3 (as illustrated by Fig. 12). As a result, an enrichment of NH_4^+ in the coarse mode

384   (>2.1 μm) was observed during the dust storm and transition period when dust particles were

385   dominant (Fig. 6). These kinds of phenomena are different from the cases in the East Asia

386 continental outflow region including Japan Sea (Massling, et al., 2007), northern Pacific (Sullivian

387 et al., 2007) and northwestern America (Fairlie et al., 2010), where in the presence of Asian dust

388 ammonium is often enriched in fine particles as ammonium sulfate and/or ammonium bisulfate,

389 which are formed by heterogeneous reactions of sulfuric acid with ammonia, although nitrate is still

390 in coarse mode. Such differences indicate an infant state of chemical evolution of dust particles in

391 Xi'an, which is near the dust source regions.

392 **4. Summary and conclusions**

393 High time resolution of TSP and size-resolved samples in Xi'an, inland China during a dust

394 episode occurring in the March of 2013 were collected and categorized as three groups, i.e., dust

395 storm, transition and non-dust storm samples, based on the TSP levels and air parcel movement

396 tracks. Nitrate in the TSP samples only showed a strong linear correlation with ammonium during

397 the whole sampling period. On the contrary, SO_4^- and Cl^- well correlated with Na^+, Ca^{2+}, Mg^{2+} and

398 K^+ but not correlated with ammonium especially in the dust storm and transition periods. Size

399 distribution pattern of NO_3^- is similar to that of NH_4^+, which presented a bimodal pattern with a

400 dominant peak in the coarse mode when dust storm occurred and with a predominant peak in the

401 fine mode in the absence of dust storm. In the event size distribution patterns Cl^- and SO_4^- are

402 similar to those of Na^+, Ca^{2+}, Mg^{2+} and K^+, dominating in the coarse mode. During the non-event

403 Cl^-, K^+ and SO_4^- showed an increase in the fine mode due to enhancements of biomass burning

404 emission and secondary oxidation. Based on the above correlations and size distribution pattern, we

405 assumed that NO_3^-, SO_4^{2-} and Cl^- in the airborne particles during the whole campaign possibly

406 existed as NH_4NO_3, Na_2SO_4, $CaSO_4$, $MgSO_4$, K_2SO_4 and $NaCl$. Molar ratio of NO_3^-/SO_4^{2-} was

407 observed to continuously increase from less than 0.1 at the moment of the dust storm peak arrived

408 in the city to about 2.5 during the non-dust storm event, demonstrating that nitrate production is

409 much faster than sulfate. Secondarily produced NH_4^+ and NO_3^- accounted for 54±20% and 60±23%

410 of the total in the dust storm period, 87±4.0% and 91±3.0% of the total in the transition period and

411   94±2.0% and 96±1.0% of the total in the non-dust storm period, respectively. On contrast,

412   secondarily produced SO_4^{2-} is almost zero in the dust storm period and accounted for 5.0±6.0% of

413   the total at the transition time and 21±15 % of the total in the non-dust storm period. Sulfate in the

414   dust storm period is almost entirely transported from Gobi desert surface soil as chemical forms of

415   Na_2SO_4 and $CaSO_4$ that are common minerals in the desert region. Our observation results also

416   indicate that in the presence of dust storm, particles that contain hygroscopic NaCl and Na_2SO_4 can

417   take up water vapor and form a liquid phase on the particle surface, which results in the formation

418   of nitrate and the subsequent absorption of ammonia to form NH_4NO_3. Therefore, a coarse mode of

419   NH_4^+ was observed during the dust storm period. These phenomena not only demonstrate a faster

420   production of nitrate than sulfate but also indicate an infant state of chemical evolution of East

421   Asian dust particles in the regions near the source.

422

427

428   **Reference**
429   Andreae, M. O., T. W. Andreae, H. Annegarn, J. Beer, H. Cachier, P. leCanut, W. Elbert, W. Maenhaut, I. Salma, F. G.
430   Wienhold, and T. Zenker: Airborne studies of aerosol emissions from savanna fires in southern Africa: 2. Aerosol
431   chemical composition, Journal of Geophysical Research, 103(D24), doi:10.1029/1098JD00107, 32119-32128, 1998.
432   Andreae, M. O., and D. Rosenfeld: Aerosol-cloud-precipitation interactions. Part 1. The nature and sources of cloud-
433   active aerosols, Earth-Science Reviews, 89(1-2), 13-41, 2008.
434   Arimoto, R., X. Y. Zhang, B. J. Huebert, C. H. Kang, D. L. Savoie, J. M. Prospero, S. K. Sage, C. A. Schloesslin, H. M.
435   Khaing, and S. N. Oh: Chemical composition of atmospheric aerosols from Zhenbeitai, China, and Gosan, South
436   Korea, during ACE-Asia, Journal of Geophysical Research-Atmospheres, 109 (D19S04),
437   doi:10.1029/2003JD004323, 2004.
438   Arimoto, R., Y. J. Kim, Y. P. Kim, P. K. Quinn, T. S. Bates, T. L. Anderson, S. Gong, I. Uno, M. Chin, B. J. Huebert,
439   A. D. Clarke, Y. Shinozuka, R. J. Weber, J. R. Anderson, S. A. Guazzotti, R. C. Sullivan, D. A. Sodeman, K. A.
440   Prather, and I. N. Sokolik: Characterization of Asian Dust during ACE-Asia, Global and Planetary Change, 52, 23-
441   56, 2006.
442   Boreddy, S. K. R., K. Kawamura, and J. Jung: Hygroscopic properties of particles nebulized from water extracts of
443   aerosols collected at Chichijima Island in the western North Pacific: An outflow region of Asian dust, Journal of
444   Geophysical Research: Atmospheres, 119(1), 2013JD020626, 2014.
445   Boyd, P. W., T. Jickells, C. S. Law, S. Blain, E. A. Boyle, K. O. Buesseler, K. H. Coale, J. J. Cullen, H. J. W. de Baar,
446   M. Follows, M. Harvey, C. Lancelot, M. Levasseur, N. P. J. Owens, R. Pollard, R. B. Rivkin, J. Sarmiento, V.
447   Schoemann, V. Smetacek, S. Takeda, A. Tsuda, S. Turner, and A. J. Watson: Mesoscale Iron Enrichment
448   Experiments 1993-2005: Synthesis and Future Directions, Science, 315(5812), 612-617, 2007.
449   Buseck, P. R., and M. Pósfai: Airborne minerals and related aerosol particles: Effects on climate and the environment,
450   Proceedings of the National Academy of Sciences, 96(7), 3372-3379, 1999.
451   Cape, J. N., S. E. Cornell, T. D. Jickells, and E. Nemitz: Organic nitrogen in the atmosphere — Where does it come
452   from? A review of sources and methods, Atmospheric Research, 102, 30–48, 2011.
453   China Statistical Press (2012), China Statistical Yearbook, edited, Chinese Statistics Press, Beijing.

454 Chen, H. Y., L. D. Chen, Z. Y. Chiang, C. C. Hung, F. J. Lin, W. C. Chou, G. C. Gong, and L. S. Wen: Size
455   fractionation and molecular composition of water-soluble inorganic and organic nitrogen in aerosols of a coastal
456   environment, Journal of Geophysical Research-Atmospheres, 115, D22307, doi:22310.21029/22010JD014157, 2010.
457 Creamean, J. M., K. J. Suski, D. Rosenfeld, A. Cazorla, P. J. DeMott, R. C. Sullivan, A. B. White, F. M. Ralph, P.
458   Minnis, J. M. Comstock, J. M. Tomlinson, and K. A. Prather: Dust and Biological Aerosols from the Sahara and
459   Asia Influence Precipitation in the Western U.S, Science, 339(6127), 1572-1578, 2013.
460 Duce, R. A., J. LaRoche, K. Altieri, K. R. Arrigo, A. R. Baker, D. G. Capone, S. Cornell, F. Dentener, J. Galloway, R.
461   S. Ganeshram, R. J. Geider, T. Jickells, M. M. Kuypers, R. Langlois, P. S. Liss, S. M. Liu, J. J. Middelburg, C. M.
462   Moore, S. Nickovic, A. Oschlies, T. Pedersen, J. Prospero, R. Schlitzer, S. Seitzinger, L. L. Sorensen, M. Uematsu,
463   O. Ulloa, M. Voss, B. Ward, and L. Zamora: Impacts of Atmospheric Anthropogenic Nitrogen on the Open Ocean,
464   Science, 320, 893-897,doi810.1126/science.1150369, 2008.
465 Fairlie, T. D., D. J. Jacob, J. E. Dibb, B. Alexander, M. A. Avery, A. v. Donkelaar, and L. Zhang: Impact of mineral
466   dust on nitrate, sulfate, and ozone in transpacific Asian pollution plumes, Atmos. Chem. Phys., 10, 3999-4012, 2010.
467 Finlayson-Pitts, B. J., L. M. Wingen, A. L. Sumner, D. Syomin, and K. A. Ramazan: The heterogeneous hydrolysis of
468   NO_2 in laboratory systems and in outdoor and indoor atmospheres: An integrated mechanism, Physical Chemistry
469   Chemical Physics, 5(2), 223-242, 2003.
470 Formenti, P., L. Schütz, Y. Balkanski, K. Desboeufs, M. Ebert, K. Kandler, A. Petzold, D. Scheuvens, S. Weinbruch,
471   and D. Zhang: Recent progress in understanding physical and chemical properties of African and Asian mineral dust,
472   Atmos. Chem. Phys., 11(16), 8231-8256, 2011.
473 Geng, H., H. Hwang, X. Liu, S. Dong, and C. U. Ro: Investigation of aged aerosols in size-resolved Asian dust storm
474   particles transported from Beijing, China, to Incheon, Korea, using low-Z particle EPMA, Atmos. Chem. Phys.,
475   14(7), 3307-3323, 2014.
476 Grassian, V. H.: Heterogeneous uptake and reaction of nitrogen oxides and volatile organic compounds on the surface
477   of atmospheric particles including oxides, carbonates, soot and mineral dust: Implications for the chemical balance
478   of the troposphere, International Reviews in Physical Chemistry, 20(3), 467-548, 2001.
479 Hanisch, F., and J. N. Crowley: The heterogeneous reactivity of gaseous nitric acid on authentic mineral dust samples,
480   and on individual mineral and clay mineral components, Physical Chemistry Chemical Physics, 3(12), 2474-2482,
481   2001.
482 He, H.: Mineral dust and NOx promote the conversion of SO_2 to sulfate in heavy pollution days, Scientific Reports, 4,
483   4172-4176, 2014.
484 Hinds, W. C. (1999), *Aerosol Technology: Properties, behavior, and measurement of airborne particles*, John Willy &
485   Sons, New York.
486 Huang, K., G. Zhuang, J. Li, Q. Wang, Y. Sun, Y. Lin, and J. S. Fu: Mixing of Asian dust with pollution aerosol and
487   the transformation of aerosol components during the dust storm over China in spring 2007, Journal Geophysical
488   Research-Atmospheres, 115, D00K13, doi:10.1029/2009JD013145, 2010.
489 Huang, K., G. Zhuang, Q. Wang, J. S. Fu, Y. Lin, T. Liu, L. Han, and C. Deng: Extreme haze pollution in Beijing
490   during January 2013: chemical characteristics, formation mechanism and role of fog processing, Atmos. Chem. Phys.
491   Discuss., 14(6), 7517-7556, 2014.
492 Huang, Y. and G. H. Wang. Hourly variations of composition and hygroscopicity of ambient particles in Xi'an during
493   dust storm periods. Journal of Earth Environment (in Chinese), 2014.
494 Huebert, B. J., T. Bates, P. B. Russell, G. Y. Shi, Y. J. Kim, K. Kawamura, G. Carmichael, and T. Nakajima: An
495   overview of ACE-Asia: Strategies for quantifying the relationships between Asian aerosols and their climatic
496   impacts, Journal of Geophysical Research-Atmospheres, 108(D23), 8663, doi:8610.1029/2003JD003550, 2003.
497 Jickells, T. D., Z. S. An, K. K. Andersen, A. R. Baker, G. Bergametti, N. Brooks, J. J. Cao, P. W. Boyd, R. A. Duce, K.
498   A. Hunter, H. Kawahata, N. Kubilay, J. laRoche, P. S. Liss, N. Mahowald, J. M. Prospero, A. J. Ridgwell, I. Tegen,
499   and R. Torres: Global Iron Connections Between Desert Dust, Ocean Biogeochemistry, and Climate, Science,
500   308(5718), 67-71, 2005.
501 Kanakidou, M., R. A. Duce, J. M. Prospero, A. R. Baker, C. Benitez-Nelson, F. J. Dentener, K. A. Hunter, P. S. Liss, N.
502   Mahowald, G. S. Okin, M. Sarin, K. Tsigaridis, M. Uematsu, L. M. Zamora, and T. Zhu: Atmospheric fluxes of
503   organic N and P to the global ocean, Global Biogeochemical Cycles, 26(3), GB3026, 2012.
504 Kim, Y. S., Y. Iwasaka, G. Y. Shi, T. Nagatani, T. Shibata, D. Trochkin, A. Matsuki, M. Yamada, B. Chen, D. Zhang,
505   M. Nagatani, and H. Nakata: Dust particles in the free atmosphere over desert areas on the Asian continent:
506   Measurements from summer 2001 to summer 2002 with balloon-borne optical particle counter and lidar, Dunhuang,
507   China, Journal of Geophysical Research-Atmospheres, 109(D19), 2004.
508 Laskin, A., T. W. Wietsma, B. J. Krueger, and V. H. Grassian: Heterogeneous chemistry of individual mineral dust
509   particles with nitric acid: A combined CCSEM/EDX, ESEM, and ICP-MS study, Journal of Geophysical Research:
510   Atmospheres, 110(D10), D10208, 2005.
511 Leaitch, W. R., A. M. Macdonald, K. G. Anlauf, P. S. K. Liu, D. Toom-Sauntry, S.-M. Li, J. Liggio, K. Hayden, M.
512   A.Wasey, L. M. Russell, S. Takahama, S. Liu, A. v. Donkelaar, T. Duck, R. V. Martin, Q. Zhang, Y. Sun, I.
513   McKendry, N. C. Shantz, and M. Cubison: Evidence for Asian dust effects from aerosol plume measurements

514   during INTEX-B 2006 near Whistler, BC, Atmos. Chem. Phys., 9, 3523-3546, 2009.

515   Li, G., J. Chen, Y. Chen, J. Yang, J. Ji, and L. Liu: Dolomite as a tracer for the source regions of Asian dust, Journal of
516   Geophysical Research: Atmospheres, 112(D17), D17201, 2007.

517   Li, W. J., and L. Y. Shao: Observation of nitrate coatings on atmospheric mineral dust particles Atmos. Chem. Phys., 9,
518   1863-1871, 2009.

519   Li, W., L. Shao, Z. Shi, J. Chen, L. Yang, Q. Yuan, C. Yan, X. Zhang, Y. Wang, J. Sun, Y. Zhang, X. Shen, Z. Wang,
520   and W. Wang: Mixing state and hygroscopicity of dust and haze particles before leaving Asian continent, Journal of
521   Geophysical Research: Atmospheres 119 (2), 1044-1059, 2014.

522   Liu, T.: Loess in China, China Ocean Press, Beijing, 1985.

523   Lu, Z., D. G. Streets, Q. Zhang, S. Wang, G. R. Carmichael, Y. F. Cheng, C. Wei, M. Chin, T. Diehl, and Q. Tan:
524   Sulfur dioxide emissions in China and sulfur trends in East Asia since 2000, Atmos. Chem. Phys., 10(13), 6311-
525   6331, 2010.

526   Maher, B. A., T. J. Mutch, and D. Cunningham: Magnetic and geochemical characteristics of Gobi Desert surface
527   sediments: Implications for provenance of the Chinese Loess Plateau Geology, 37, 279-282, 2009.

528   Manktelow, P. T., K. S. Carslaw, G. W. Mann, and D. V. Spracklen: The impact of dust on sulfate aerosol, CN and
529   CCN, Atmos. Chem. Phys., 10, 365-382, 2010.

530   Massling, A., S. Leinert, A. Wiedensohler, and D. Covert: Hygroscopic growth of sub-micrometer and one-micrometer
531   aerosol particles measured during ACE-Asia, Atmos. Chem. Phys., 7, 3249–3259, 2007.

532   McNaughton, C. S., A. D. Clarke, V. Kapustin, Y. Shinozuka, S. G. Howell, B. E. Anderson, E. Winstead, J. Dibb, E.
533   Scheuer, R. C. Cohen, P. Wooldridge, A. Perring, L. G. Huey, S. Kim, J. L. Jimenez, E. J. Dunlea, P. F. DeCarlo, P.
534   O. Wennberg, J. D. Crounse, A. J. Weinheimer, and F. Flocke: Observations of heterogeneous reactions between
535   Asian pollution and mineral dust over the Eastern North Pacific during INTEX-B, Atmos. Chem. Phys., 9, 8283-
536   8308, 2009.

537   Menon, S., N. Unger, D. Koch, J. Francis, T. Garrett, I. Sednev, D. Shindell, and D. Streets: Aerosol climate effects and
538   air quality impacts from 1980 to 2030, Environ. Res. Lett., 3(2), 2008.

539   Mochida, M., N. Umemoto, K. Kawamura, H. Lim, and B. J. Turpin: Bimodal size distributions of various organic
540   acids and fatty acids in the marine atmosphere: Influence of anthropogenic aerosols, Asian dusts, and sea spray off
541   the coast of East Asia, J. Geophys. Res., 112, D15209, doi:15210.11029/12006JD007773, 2007.

542   Mogili, P. K., P. D. Kleiber, M. A. Young, and V. H. Grassian: N2O5 hydrolysis on the components of mineral dust
543   and sea salt aerosol: Comparison study in an environmental aerosol reaction chamber, Atmospheric Environment,
544   40(38), 7401-7408, 2006.

545   Nie, W., T. Wang, L. K. Xue, A. J. Ding, X. F. Wang, X. M. Gao, Z. Xu, Y. C. Yu, C. Yuan, Z. S. Zhou, R. Gao, X. H.
546   Liu, Y. Wang, S. J. Fan, S. Poon, Q. Z. Zhang, and W. X. Wang: Asian dust storm observed at a rural mountain site
547   in southern China: chemical evolution and heterogeneous photochemistry, Atmos. Chem. Phys., 12(24), 11985-
548   11995, 2012.

549   Parrington, J. R., W. H. Zoller, and N. K. Aras: Asian dust: Seasonal transport to the Hawaiian Islands, Science, 220,
550   195-197, 1983.

551   Pathak, R. K., T. Wang, and W. S. Wu: Nighttime enhancement of PM2.5 nitrate in ammonia-poor atmospheric
552   conditions in Beijing and Shanghai: Plausible contributions of heterogeneous hydrolysis of N_2O_5 and HNO_3
553   partitioning, Atmospheric Environment, 45, 1183-1191, 2011.

554   Saliba, N. A., and A. Chamseddine: Uptake of acid pollutants by mineral dust and their effect on aerosol solubility,
555   Atmospheric Environment, 46, 256-263, 2012.

556   Seinfeld, J. H., G. R. Carmichael, R. Arimoto, W. C. Conant, F. J. Brechtel, T. A. Bates, T. A. Cahill, A. D. Clarke, S. J.
557   Doherty, P. J. Flatau, B. J. Huebert, J. Kim, K. M. Markowicz, P. K. Quinn, L. M. Russell, P. B. Russell, A. Shimizu,
558   Y. Shinozuka, C. H. Song, Y. H. Tang, I. Uno, A. M. Vogelmann, R. J. Weber, J. H. Woo, and X. Y. Zhang:
559   ACEAsia: Regional climatic and atmospheric chemical effects of Asian dust and pollution, Bulletin of American
560   Meteorological Society, 85, 367-380, doi:310.1175/BAMS-1185-1173-1367, 2004.

561   Shen, Z. X., J. J. Cao, R. Arimoto, R. J. Zhang, D. M. Jie, S. X. Liu, and C. S. Zhu: Chemical composition and source
562   characterization of spring aerosol over Horqin sand land in northeastern China, Journal of Geophysical Research-
563   Atmospheres, 112 (D14315), doi:10.1029/2006JD007991, 2007.

564   Shen, Z., R. Arimoto, J. Cao, R. Zhang, X. Li, N. Du, T. Okuda, S. Nakao, and S. Tanaka: Seasonal Variations and
565   evidence for the effectiveness of pollution controls on water-soluble inorganic species in total suspended particulates
566   and fine particulate patter from Xi'an, China, Journal of the Air & Waste Management Association, 58(12), 1560-
567   1570, 2008.

568   Singh, H. B., W. H. Brune, J. H. Crawford, F. Flocke, and D. J. Jacob: Chemistry and transport of pollution over the
569   Gulf of Mexico and the Pacific: spring 2006 INTEX-B campaign overview and first results, Atmos. Chem. Phys.,
570   9(7), 2301-2318, 2009.

571   Song, Y. C., H. J. Eom, H. J. Jung, M. A. Malek, H. K. Kim, H. Geng, and C. U. Ro: Investigation of aged Asian dust
572   particles by the combined use of quantitative ED-EPMA and ATR-FTIR imaging, Atmos. Chem. Phys., 13(6),
573   3463-3480, 2013.

574 Sullivan, R. C., and K. A. Prather: Investigations of the diurnal cycle and mixing state of oxalic acid in individual
575   particles in Asian aerosol outflow, Environmental Science & Technology, 41(23), 8062-8069, 2007.
576 Sullivan, R. C., M. J. K. Moore, M. D. Petters, S. M. Kreidenweis, G. C. Roberts, and K. A. Prather: Effect of chemical
577   mixing state on the hygroscopicity and cloud nucleation properties of calcium mineral dust particles, Atmospheric
578   Chemistry and Physics, 9, 3303–3316, 2009.
579 Sullivan, R. C., M. J. K. Moore, M. D. Petters, S. M. Kreidenweis, G. C. Roberts, and K. A. Prather: Timescale for
580   hygroscopic conversion of calcite mineral particles through heterogeneous reaction with nitric acid, Phys. Chem.
581   Chem. Phys., 11(36), 7826-7837, 2009.
582 Sullivian, R. C., S. A. Guazzotti, D. A. Sodeman, and K. A. Prather: Direct observations of the atmospheric processing
583   of Asian mineral dust, Atmos. Chem. Phys., 7, 1213-1236, 2007.
584 Sun, Y., G. Zhuang, K. Huang, J. Li, Q. Wang, Y. Wang, Y. Lin, J. S. Fu, W. Zhang, A. Tang, and X. Zhao: Asian dust
585   over northern China and its impact on the downstream aerosol chemistry in 2004, J. Geophys. Res., 115,
586   D00K09,doi:10.1029/2009jd012757, 2010.
587 Takahashi, Y., M. Higashi, T. Furukawa, and S. Mitsunobu: Change of iron species and iron solubility in Asian dust
588   during the long-range transport from western China to Japan, Atmos. Chem. Phys., 11(21), 11237-11252, 2011.
589 Tobo, Y., D. Zhang, A. Matsuki, and Y. Iwasaka: Asian dust particles converted into aqueous droplets under remote
590   marine atmospheric conditions, Proceedings of National Academy of Science of United States of America, 107,
591   17905-17910, 2010.
592 Uno, I., K. Eguchi, K. Yumimoto, T. Takemura, A. Shimizu, M. Uematsu, Z. Y. Liu, Z. F. Wang, Y. Hara, and N.
593   Sugimoto: Asian dust transported one full circuit around the globe, Nat. Geosci., 2, 557–560, 2009.
594 Usher, C. R., A. E. Michel, and V. H. Grassian: Reactions on mineral dust, Chem. Rev. , 103, 4883-4939, 2003. van
595   Donkelaar, A., R. V. Martin, M. Brauer, R. Kahn, R. Levy, C. Verduzco, and P. J. Villeneuve: Global estimates of
596   ambient fine particulate matter concentrations from satellite-based aerosol optical depth: development and
597   application, Environmental Health Perspectives, 118, 8347-8355, 2010.
598 Wang, G., M. Xie, S. Hu, E. Tachibana, and K. Kawamura: Dicarboxylic acids, metals and isotopic compositions of C
599   and N in atmospheric aerosols from inland China: Implications for dust and coal burning emission and secondary
600   aerosol formation, Atmospheric Chemistry and Physics, 10, 6087-6096, 2010.
601 Wang, G., J. Li, C. Chen, S. Hu, M. Xie, S. Gao, B. Zhou, W. Dai, J. Cao, and Z. An: Observation of atmospheric
602   aerosols at Mt. Hua and Mt. Tai in central and east China during spring 2009-Part 1. EC, OC and inorganic ions,
603   Atmospheric Chemistry and Physics, 11, 4221-4235, 2011.
604 Wang, G. H., B. H. Zhou, C. L. Cheng, J. J. Cao, J. J. Li, J. J. Meng, J. Tao, R. J. Zhang, and P. Q. Fu: Impact of Gobi
605   desert dust on aerosol chemistry of Xi'an, inland China during spring 2009: differences in composition and size
606   distribution between the urban ground surface and the mountain atmosphere, Atmos. Chem. Phys., 13(2), 819-835,
607   2013.
608 Wang, G. H., J. J. Li, C. L. Cheng, B. H. Zhou, M. J. Xie, S. Y. Hu, J. J. Meng, T. Sun, Y. Q. Ren, J. J. Cao, S. X. Liu,
609   T. Zhang, and Z. Z. Zhao: Observation of atmospheric aerosols at Mt. Hua and Mt. Tai in central and east China
610   during spring 2009-Part 2. Impact of dust storm on organic aerosol composition and size distribution, Atmos. Chem.
611   Phys., 12, 4065-4080, 2012.
612 Wang, S. W., Q. Zhang, D. G. Streets, K. B. He, R. V. Martin, L. N. Lamsal, D. Chen, Y. Lei, and Z. Lu: Growth in
613   NOx emissions from power plants in China: bottom-up estimates and satellite observations, Atmos. Chem. Phys., 12,
614   4429–4447, 2012.
615 Wang, Y., Q. Q. Zhang, K. He, Q. Zhang, and L. Chai: Sulfate-nitrate-ammonium aerosols over China: response to
616   2000–2015 emission changes of sulfur dioxide, nitrogen oxides, and ammonia, Atmos. Chem. Phys., 13(5), 2635-
617   2652, 2013.
618 Wang, Y. H., B. Hu, D. S. Ji, Z. R. Liu, G. Q. Tang, J. Y. Xin, H. X. Zhang, T. Song, L. L. Wang, W. K. Gao, X. K.
619   Wang, and Y. S. Wang: Ozone weekend effects in the Beijing–Tianjin–Hebei metropolitan area, China, Atmos.
620   Chem. Phys., 14(5), 2419-2429, 2014.
621 Wu, F., D. Zhang, J. Cao, H. Xu, and Z. An: Soil-derived sulfate in atmospheric dust particles at Taklimakan desert,
622   Geophysical Research Letters, 39, L24803, doi:24810.21029/22012GL054406,, 2012.
623 Zamora, L. M., J. M. Prospero, and D. A. Hansell: Organic nitrogen in aerosols and precipitation at Barbados and
624   Miami: Implications regarding sources, transport and deposition to the western subtropical North Atlantic, Journal
625   of Geophysical Research, 116,, D20309, doi:20310.21029/22011JD015660, 2011.
626 Zamora, L. M., J. M. Prospero, D. A. Hansell, and J. M. Trapp: Atmospheric P deposition to the subtropical North
627   Atlantic: sources, properties, and relationship to N deposition, Journal of Geophysical Research: Atmospheres,
628   118(3), 1546-1562, doi:1510.1002/jgrd.50187, 2013.
629 Zhang, Q., D. G. Streets, G. R. Carmichael, K. B. He, H. Huo, A. Kannari, Z. Klimont, I. S. Park, S. Reddy, J. S. Fu, D.
630   Chen, L. Duan, Y. Lei, L. T. Wang, and Z. L. Yao: Asian emissions in 2006 for the NASA INTEX-B mission,
631   Atmos. Chem. Phys., 9(14), 5131-5153, 2009.
632 Zheng, X.: Salt lakes on the Inner Mongolian plateau of China, Chinese Geographic Science, 1, 83-94, 1991.
633

634   **Table List**

635   Table 1. Meteorological parameters and hourly concentrations of gaseous pollutants, inorganic ions,
636   elements, EC, OC, TSP and other water-soluble species during the dust storm, transition
637   and non-dust storm periods.
638
639   Table 2. Accumulative percentages (%) of mass concentrations of major ions on the 9-stage filters
640   collected in Xi'an during the spring dust storm and non-dust storm periods.
641
642   Table 3. Concentrations (μg m^{-3}) of different sulfates in the water-soluble fraction of TSP samples
643   and their relative abundances (%) to the total water-soluble sulfate during the dust storm
644   and transition periods
645
646
647   **Fig. Caption**

648
649   Fig. 1. Backward trajectories of air masses arriving in Xi'an during the campaign (**a-d**) and the
650   topography of Guanzong Basin and it's surrounding areas (**e**) (duration 48 hr, air parcels of
651   100 m, 300 m and 500m above ground level are in red, blue and green, respectively)
652
653   Fig. 2. Temporal variations of TSP, PM$_{2.5}$, EC and OC during the campaign.
654
655   Fig. 3. Comparison of relative abundance of ions, OC, EC, WSOC and WSON in the TSP samples
656   during the dust storm event, transition time and non-dust storm period.
657
658   Fig. 4. Temporal variations of inorganic ions during the campaign.
659
660   Fig. 5.Relative abundances of Ca^{2+}/Ca, Ca/TSP, SO$_4^{2-}$-S/total-S and SO$_4^{2-}$/TSP during the
661   campaign.
662
663   Fig. 6. Size distributions of major ions during the dust and non-dust storm periods.
664
665   Fig. 7. Linear fit regressions for nitrate and sulfate with ammonium and other cations in the TSP
666   samples collected during the dust storm and transition periods (red dots are the three
667   samples collected at the earliest three hours).
668
669   Fig. 8. Equivalent percentages of inorganic ions in the TSP samples during the campaign.
670
671   Fig. 9. Chemical forms of water-soluble sulfate salts in the TSP samples during the dust storm and
672   transition periods.
673
674   Fig. 10. Production speed of nitrate during the sampling period ((**a**) molar ratio of nitrate/sulfate in
675   the TSP samples and (**b**) linear fit regression for the nighttime molar ratio of nitrate/sulfate
676   with observation duration).
677
678   Fig. 11. Mass ratios of nitrate, sulfate and ammonium produced by heterogeneous reactions to the
679   totals in the TSP samples.
680
681   Fig. 12. A diagram for heterogeneous formation mechanism of ammonium nitrate on dust surface
682   in Xi'an during the dust storm event

683
684
685
686

Table 1. Meteorological parameters and hourly concentrations of inorganic ions, elements, EC, OC, water-soluble organic (WSOC) and inorganic carbon(WSIC) and water-soluble organic (WSON) and inorganic nitrogen (WSIN) in total suspended particles (TSP) during the dust storm, transition and non-dust periods

Time	Dust storm (03/09,1800− 03/10, 2100)	Transition (03/10, 2100− 03/11, 1200)	Non−dust storm (03/11,1200− 03/12, 1000)
I. Meteorological parameters and online measured PM$_{2.5}$			
Relative humidity (RH, %)	22±3.5(14−26)	53±9.0(34−64)	48 ±6.0(33−61)
Wind speed (WS, m s^{-1})	2.0±0.6(0.7−2.9)	1.6±0.7(0.7−3.5)	2.1±0.8(0.4−3.2)
Temperature (T, ^{o}C)	13±2.7(9.1−20)	5.4±1.7(3.3−8.5)	10±1.3(8.8−15)
PM$_{2.5}$, µg m^{-3}	152±127(49−621)	88±16(68−125)	150±32(119−279)
II. Inorganic ions in TSP samples, µg m^{-3}			
F$^-$	0.5±0.4(0.1−1.3)	0.6±0.3(0.2−1.3)	0.8±0.2(0.3−1.0)
Cl$^-$	5.1±6.3(1.7−34)	2.8±0.8(1.7−4.9)	4.3±2.0(1.9−11)
NO$_2^-$	0.3±0.2(0.0−0.7)	0.3±0.1(0.0−0.4)	0.2±0.1(0.0−0.3)
NO$_3^-$	8.2±2.1(4.7−12)	11±2.0(7.6−15)	28±3.5(20−34)
SO$_4^{2-}$	35±34(12−180)	14±3.3(10−20)	21±4.3(15−33)
Na$^+$	18±13(5.2−72)	8.7±1.5(5.4−11)	3.9±4.1(0.0−13)
NH$_4^+$	3.0±0.7(1.7−5.1)	3.5±1.0(2.4−5.9)	7.6±0.9(5.6−8.7)
K$^+$	1.5±0.8(0.7−4.1)	0.8±0.2(0.4−1.2)	1.4±0.5(0.9−3.0)
Mg^{2+}	1.3±0.7(0.3−3.8)	0.7±0.2(0.3−1.1)	0.7±0.3(0.3−1.4)
Ca^{2+}	10±5.9(1.7−28)	6.6±1.9(2.8−9.8)	11±2.5(6.9−15)
Subtotal	83±60(37−340)	49±8.4(36−65)	79±10(56−103)
III. Elements in TSP samples, µg m^{-3}			
S	18±11(7.9−56)	7.9±1.9(5.7−12)	13±2.2(9.3−19)
Cl	6.2±6.0(2.0−30)	2.5±1.3(1.5−6.4)	6.6±2.4(3.9−12)
K	64±39(28−195)	15±4.2(9.0−21)	20±4.6(13−33)
Ca	146±81(66−411)	45±15(26−71)	55±13(35−98)
Ti	9.7±6.0(4.3−30)	2.4±0.7(1.4−3.4)	2.5±0.6(1.8−4.8)
Mn	1.2±1.0(0.0−4.3)	0.5±0.7(0.0−2.3)	0.4±0.8(0.0−3.9)
Fe	109±69(45−346)	25±8.2(15−38)	26±7.5(15−52)
Zn	0.7±0.3(0.4−1.5)	0.9±0.6(0.4−2.6)	1.4±1.1(0.6−4.1)
Cr	0.22±0.12(0.10−0.65)	0.09±0.04(0.00−0.18)	0.10±0.03(0.03−0.16)
Ni	0.04±0.04(0.00−0.14)	0.04±0.02(0.00−0.07)	0.04±0.03(0.00−0.10)
As	0.03±0.05(0.00−0.23)	0.01±0.02(0.00−0.07)	0.04±0.07(0.00−0.27)
Br	0.00±0.00(0.00−0.02)	0.02±0.03(0.00−0.11)	0.030±0.04(0.00−0.15)
Mo	0.04±0.05(0.00−0.17)	0.04±0.06(0.00−0.19)	0.04±0.08(0.00−0.26)
Pb	0.37±0.19(0.09−0.77)	0.39±0.15(0.20−0.71)	0.39±0.12(0.14−0.65)
Subtotal[a]	506±304(193−1559)	148±42(92−225)	191±43(136−335)
IV. Other species in TSP samples, µg m^{-3}			
WSOC	15±10(4.2−52)	15±17(2.0−58)	19±11(7.8−49)
WSIC	10±2.8(6.8−20)	5.9±3.3(1.9−13)	6.0±1.7(2.9−9.5)
WSIN	4.2±1.0(2.4−6.5)	5.2±1.2(3.6−8.0)	12±1.3(9.1−14)
WSON	2.5±1.8(0.0−8.0)	1.7±0.8(0.5−3.1)	5.9±3.6(1.4−16)
OC	68±50(8.7−254)	32±9.1(20−49)	55±13(37−84)
EC	6.7±8.6(0.0−32)	7.1±2.4(3.4−12)	8.9±6.2(0.0−28)
TSP	2109±1360(774−7527)	630±155(412−1037)	687±194(476−1399)
PM$_{2.5}$/TSP, %	7.4±3.4(2.3−13)	14±2.4(9.6−18)	23±4.8(10−30)

[a]Calculated as SO$_4^{2-}$+Cl$^-$+metal oxides.

Table 2. Accumulative percentages (%) of mass concentrations of major ions on the 9-stage filters collected in Xi'an during the spring dust storm and non-dust storm periods

Size range, μm	Cl^-	NO_3^-	SO_4^{2-}	NH_4^+	Na^+	K^+	Mg^{2+}	Ca^{2+}
Dust storm period (03/09,1800−03/10,2100)								
>9.0	100	100	100	100	100	100	100	100
5.8−9.0	86±1	87±1	83±3	74±10	87±1	88±5	85±2	83±6
4.7−5.8	74±2	71±4	64±5	52±9	75±2	69±3	70±3	68±5
3.3−4.7	62±2	60±5	51±5	37±17	62±3	62±9	57±2	49±7
2.1−3.3	51±2	44±6	37±7	31±13	51±3	49±9	43±3	32±6
1.1−2.1	40±4	31±6	27±7	21±16	39±4	40±7	31±3	18±5
0.65−1.1	31±4	22±5	20±6	18±12	28±3	29±5	22±3	10±4
0.43−0.65	21±2	17±2	14±4	16±8	19±3	24±0	14±3	5±4
<0.43	11±1	9±1	7±2	9±5	9±1	11±1	7±2	2±2
Non-dust storm period (03/11,1200−03/12,2100)								
>9.0	100	100	100	100	100	100	100	100
5.8−9.0	84	80	86	77	90	93	88	91
4.7−5.8	77	75	76	73	80	86	74	77
3.3−4.7	70	70	69	72	69	80	63	64
2.1−3.3	62	64	62	69	58	74	50	48
1.1−2.1	55	58	54	65	46	66	39	35
0.65−1.1	42	42	40	46	35	46	29	25
0.43−0.65	29	25	28	27	24	28	23	22
<0.43	16	3	15	1	13	9	17	19

Table 3. Concentrations (μg m^{-3}) of different sulfates in the water-soluble fraction of TSP samples and their relative abundances (%) to the total water-soluble sulfate during the dust storm and transition periods

		K_2SO_4	$MgSO_4$	Na_2SO_4	$CaSO_4$
Dust storm period	Concentration,	3.4±1.7(1.6−9.2)	13±7.1(3.3−38)	45±30(11−155)	35±20(5.8−95)
	Relative abundance	3.6±0.7(2.5−4.7)	13±2.6(7.0−17)	47±15(21−77)	36±12(12−58)
Transition period	Concentration	1.9±0.5(0.8−2.8)	7.2±2.0(3.3−11)	21±4.0(12−25)	23±6.5(10−33)
	Relative abundance	3.0±0.8(2−5)	13±1.8(9−16)	41±9.0(26−64)	42±7.6(25−56)

Figure 1. Backward trajecotories of air masses arriving in Xi'an during the campaign (**a-d**) and the topography of Guanzong Basin and it's surrounding areas (**e**) (duration 48 hr, air parcels of 100 m,300 m and 500m above ground level are in red,blue and green)
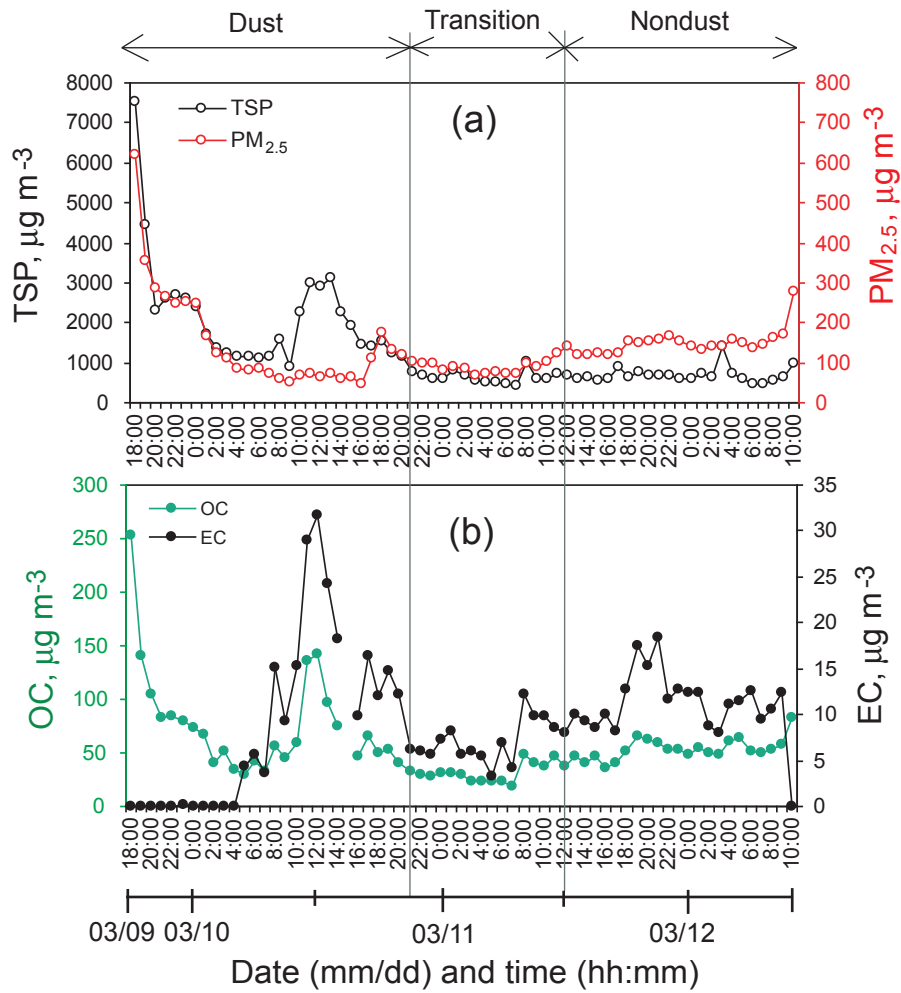
Figure 2. Temporal variations of TSP, PM2.5, EC and OC during the campaign
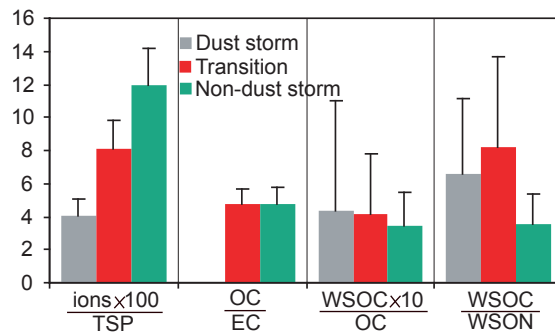
Figure 3. Comparison of relative abundance of ions, OC,EC, WSOC and WSON in the TSP samples
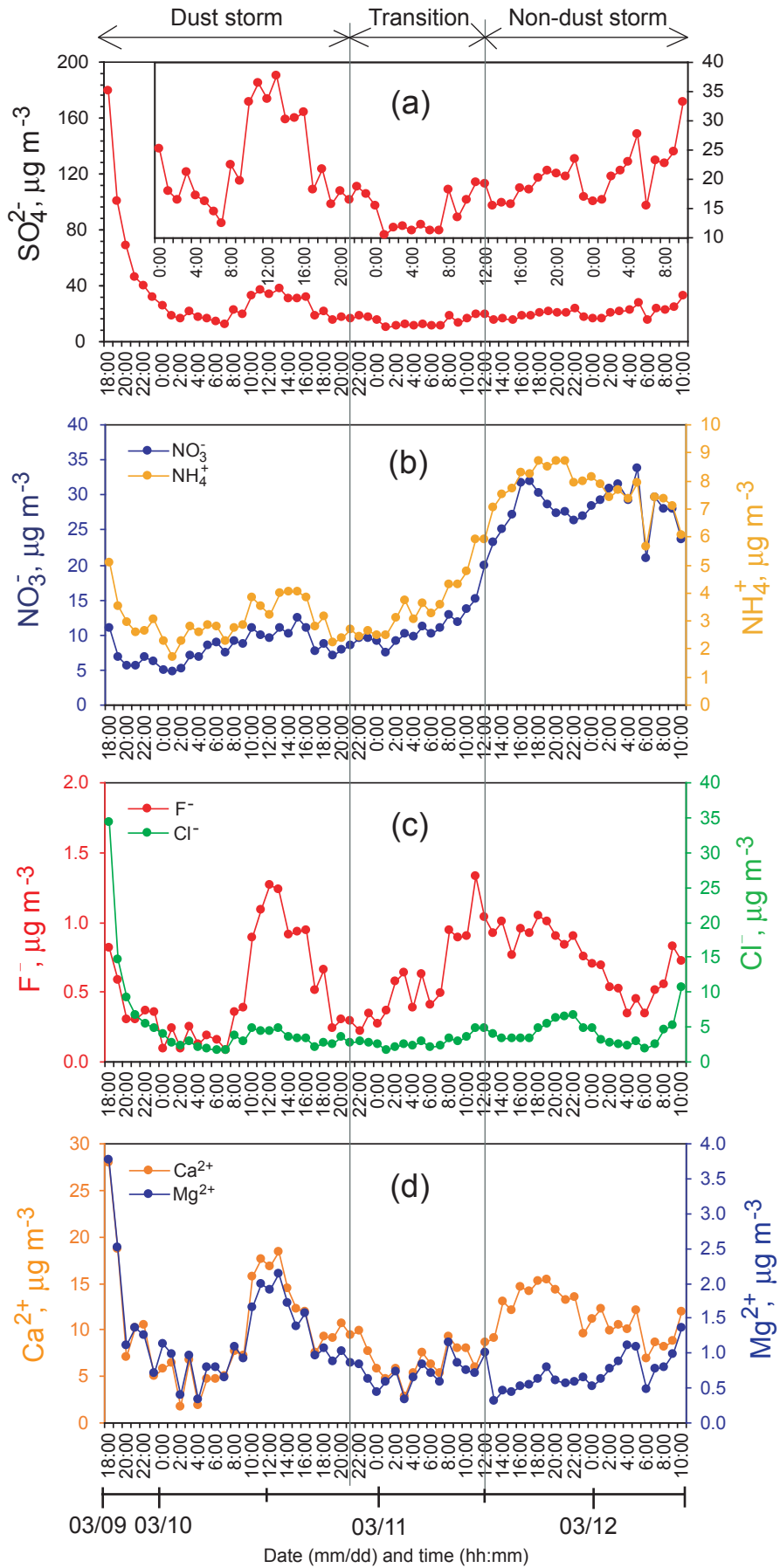
Figure 4. Temporal variations of inorganic ions during the campaign
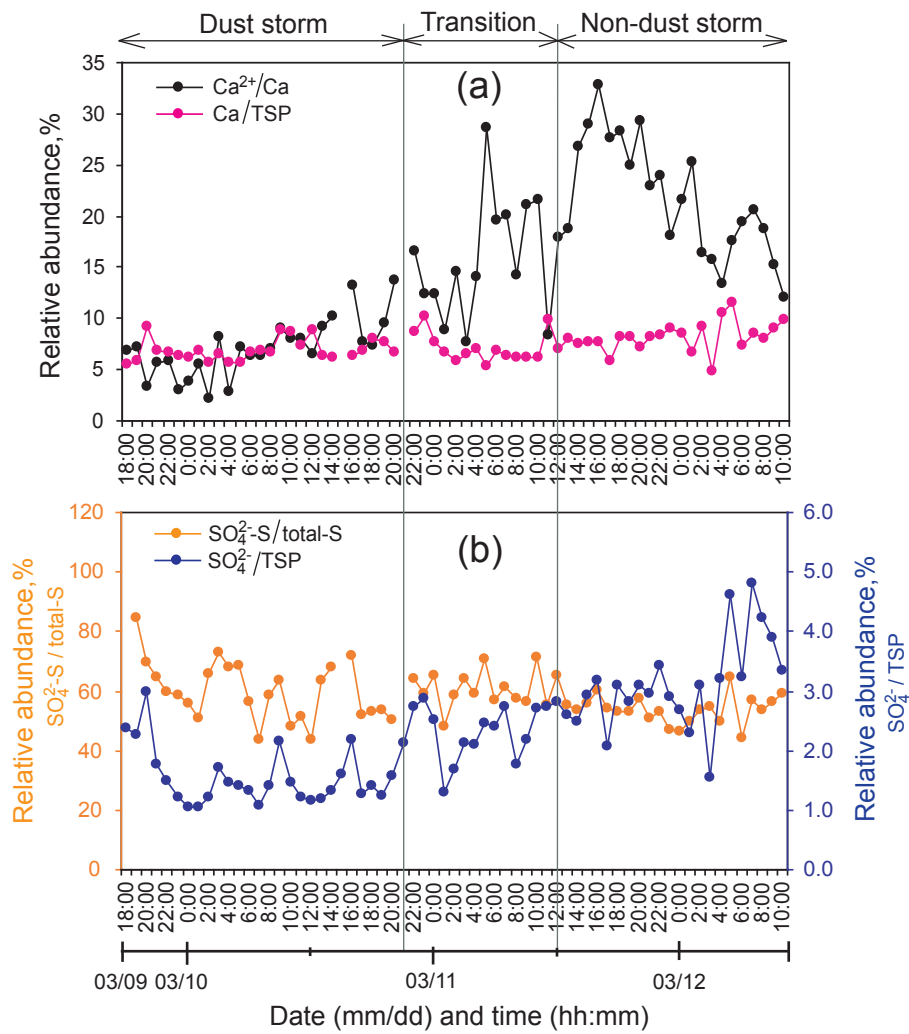
Figure 5.Relative abundances of Ca2+/Ca, Ca/TSP, SO4-S/Total S and SO42- of the TSP samples collected during the sampling periods
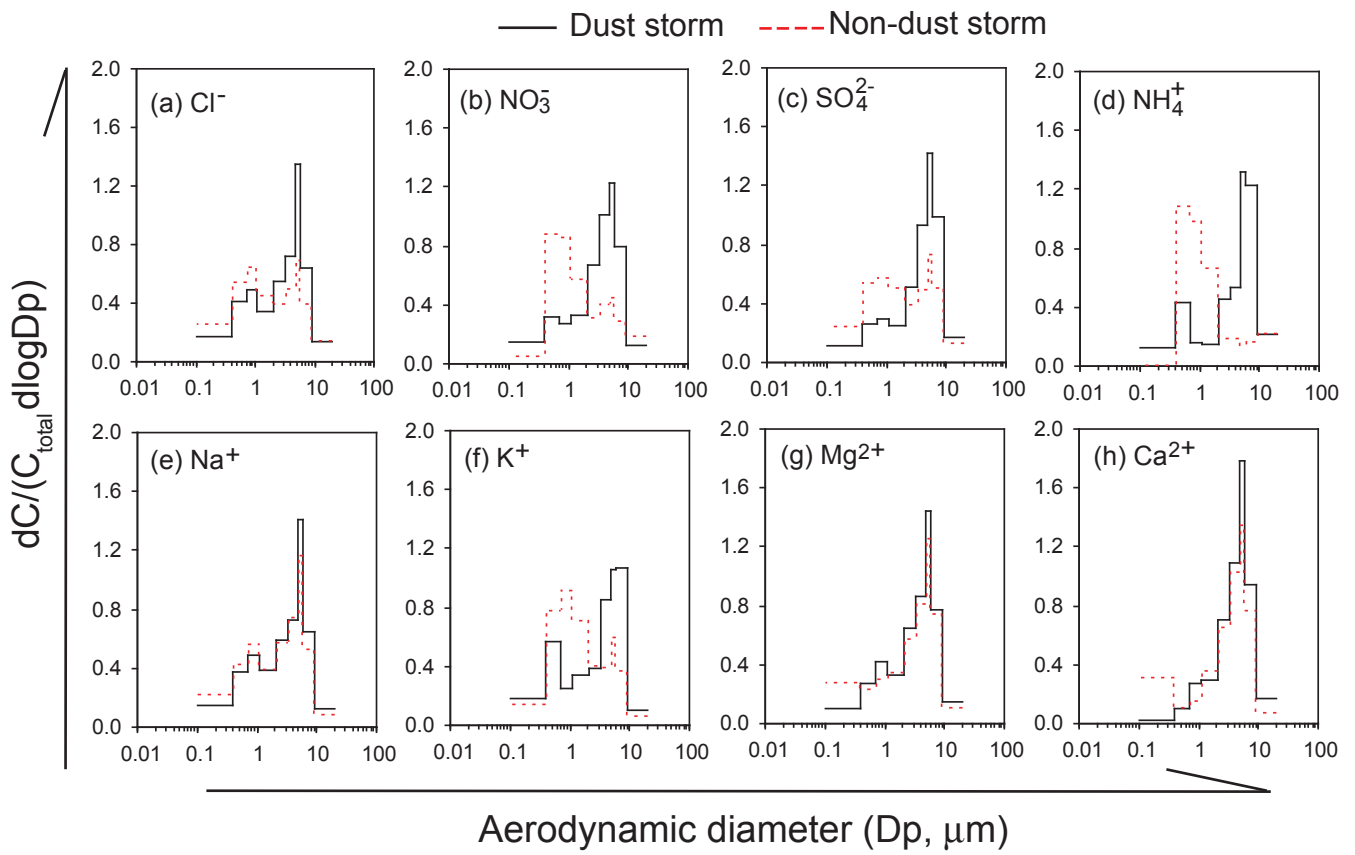
Figure 6 Size distributions of major ions during the dust storm and non-dust storm periods.
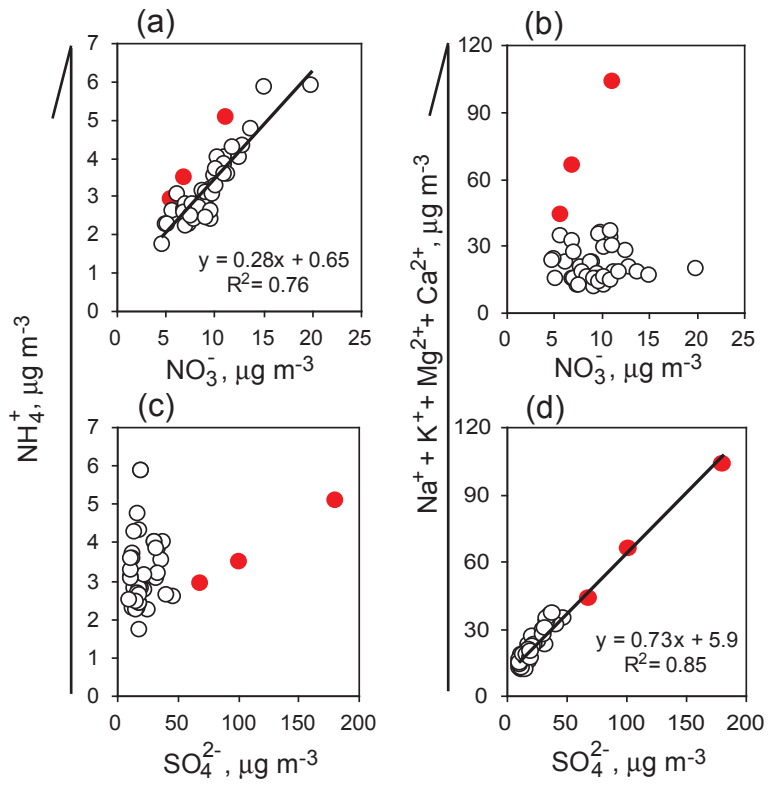
Figure 7. Linear fit regressions for nitrate and sulfate with ammonium and other cations in the TSP samples collected during the dust storm and transition periods (red dots are the three samples collected at the earliest three hours)
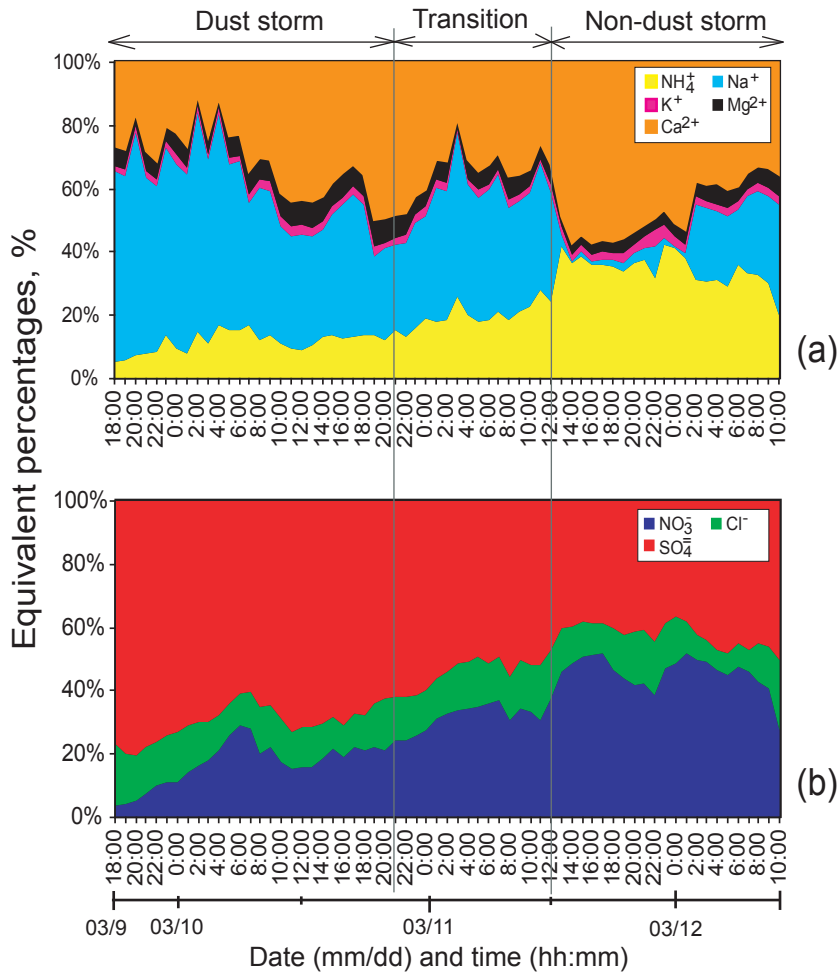
Figure 8. Equivalent percentages of inorganic ions in the TSP samples during the campaign
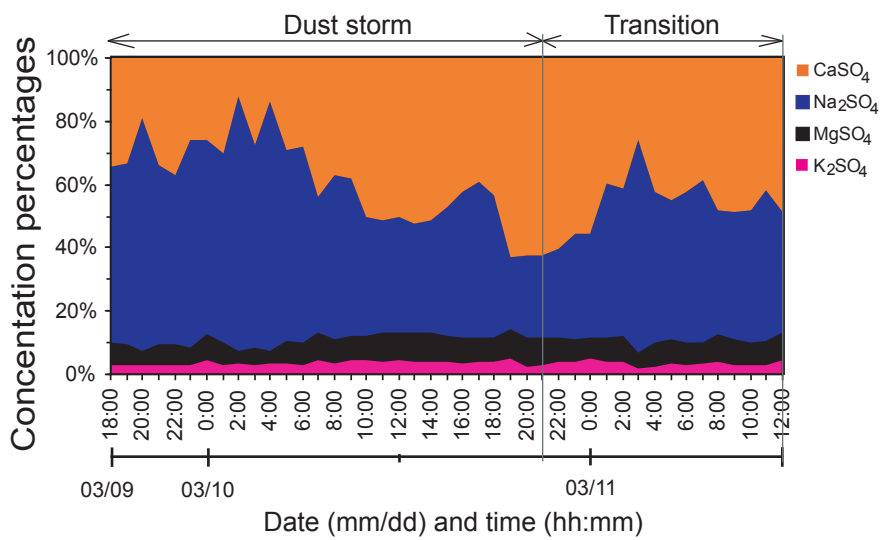
Figure 9. Chemical forms of water-souble sulfate salts in the TSP samples during the dust storm and transition periods
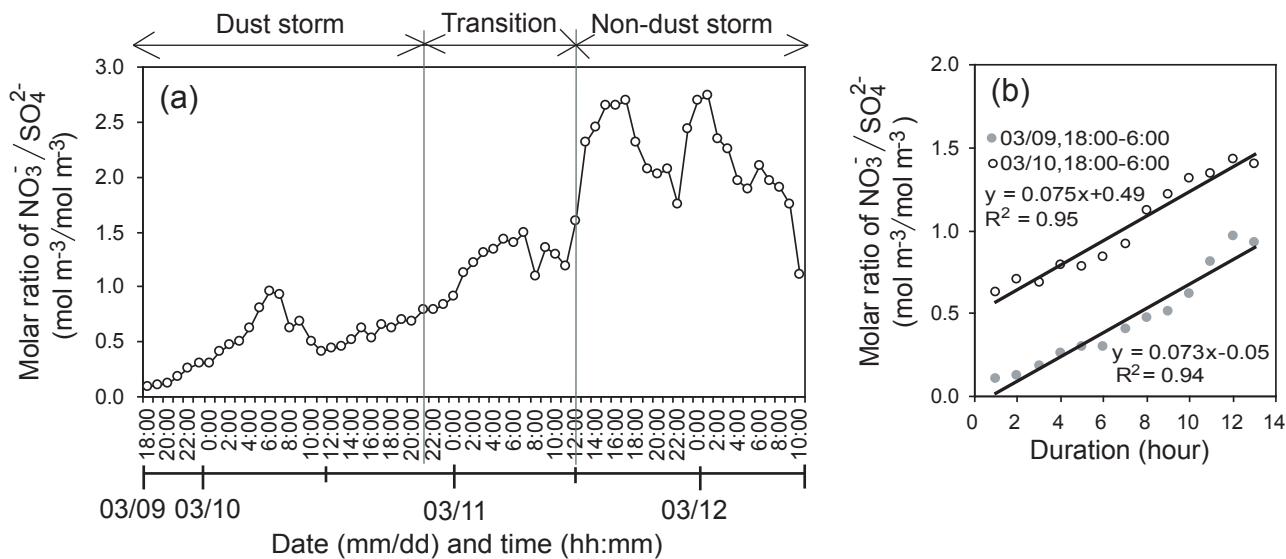
Figure 10. Production speed of nitrate during the sampling period ((a) molar ratio of nitrate/sulfate in the TSP samples and (b) linear fit regression for the nighttime molar ratio of nitrate/sulfate with observation duration).
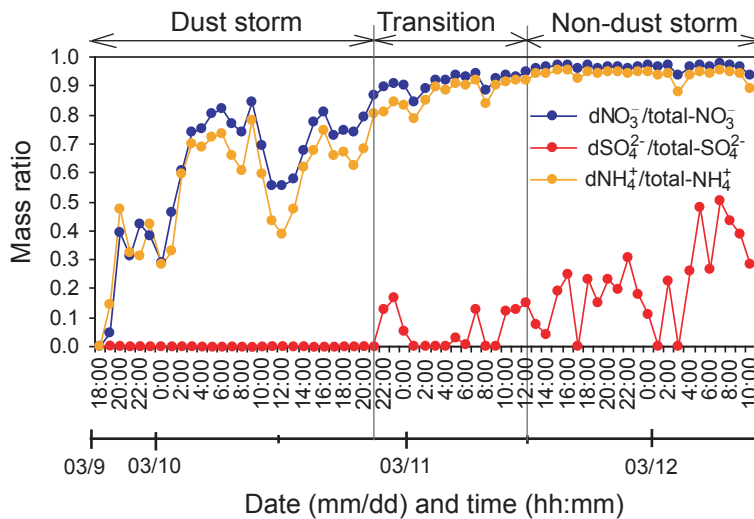
Figure 11. Mass ratios of nitrate, sulfate and ammonium produced by heterogeneous reactions to the total in the TSP samples
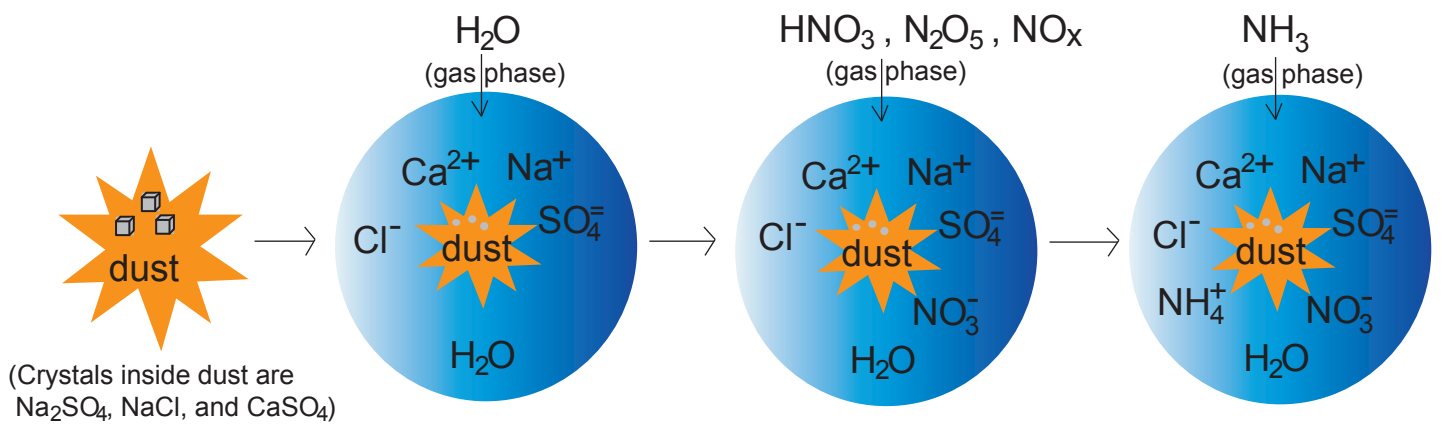
Figure 12. A diagram for heterogeneous formation mechanism of ammonium nitrate on dust surface in Xi'an during the dust storm event